HHS Public Access

Author manuscript

Magn Reson Med. Author manuscript; available in PMC 2017 March 01.

Published in final edited form as:

Magn Reson Med. 2017 March ; 77(3): 1134–1141. doi:10.1002/mrm.26200.

Volumetric Multislice GagCEST Imaging of Articular Cartilage: Optimization and Comparison with T1rho

Feliks Kogan[1,*], **Brian A. Hargreaves**[1,2,3], and **Garry E. Gold**[1,2,4]

[1]Department of Radiology, Stanford University, Stanford, CA

[2]Department of Bioengineering, Stanford University, Stanford, CA

[3]Department of Electrical Engineering, Stanford University, Stanford, CA

[4]Department of Orthopedic Surgery, Stanford University, Stanford, CA

Abstract

Purpose—To develop and optimize a multislice glycosaminoglycan (GAG) chemical exchange saturation transfer (GagCEST) sequence for volumetric imaging of articular cartilage, and to validate the sequence against $T_{1\rho}$ relaxation times in whole joint imaging of tibiotalar cartilage.

Methods—Ex vivo experiments were used to observe the effect of the number of partitions and shot TR on signal-to-noise ratio and measured $GagCEST_{asym}$. GagCEST imaging of the entire tibiotalar joint was also performed on 10 healthy subjects. The measured $GagCEST_{asym}$ was compared and correlated with $T_{1\rho}$ relaxation times.

Results—Ex vivo studies showed a higher average $GagCEST_{asym}$ from articular cartilage on multislice acquisitions acquired with two or more partitions than observed with a single-slice acquisition. In healthy human subjects, an average $GagCEST_{asym}$ of 8.8 ± 0.7% was observed. A coefficient of variation of $GagCEST_{asym}$ across slices of less than 15% was seen for all subjects. Across subjects, a Pearson correlation coefficient of −0.58 was observed between the measured $gagCEST_{asym}$ and $T_{1\rho}$ relaxation times.

Conclusions—We demonstrated the feasibility and optimization of multislice GagCEST mapping of articular cartilage. Volumetric analysis and decreased scan times will help to advance the clinical utility of GagCEST imaging of articular cartilage.

Keywords

GagCEST; GAG; cartilage; osteoarthritis

INTRODUCTION

Osteoarthritis (OA) is a chronic, degenerative disease of the joint, which causes a high degree of morbidity, including loss of mobility and pain (1,2). Despite its widespread prevalence and high cost, pathogenesis in OA is still poorly understood (3). Although OA is

*Correspondence to: Feliks Kogan, PhD, Stanford University, Department of Radiology, 1201 Welch Rd., Stanford, CA 94305. Telephone: 585-733-8684; fkogan@stanford.edu.

now widely viewed as a disease of the entire joint with many diverse etiologies, cartilage tissue degeneration is thought to be one of the predominant initiating events in the progression of OA (4,5). In its early stage, prior to measurable cartilage loss, OA is characterized by an increase in enzymatic degradation in cartilage, resulting in proteoglycan (PG) depletion (6). Proteoglycans are complex macromolecules consisting of a protein core to which many negatively charged glycosaminoglycan (GAG) side chains are attached. Detection of changes in GAG content and distribution are vital for early diagnosis of OA and potential treatment monitoring.

MRI is increasingly being used to study and evaluate early OA changes in cartilage biochemical composition (7,8). Although conventional MRI provides sufficient contrast to visualize cartilage morphology, more advanced imaging strategies are necessary for understanding the underlying biochemical composition of cartilage that begins to break down in the earliest stages of OA. These advanced quantitative techniques include delayed gadolinium-enhanced MRI of cartilage (dGEMRIC), sodium imaging, and T_1 relaxation in the rotating frame ($T_{1\rho}$) (9,10). Sodium MR imaging captures signal from positively charged sodium ions, which exist in association with the negatively charged GAG side chains (11,12). Although it is highly specific to GAG, it requires special hardware and suffers from low signal-to-noise ratio (SNR) because of the low concentration of sodium ions in cartilage and a reduced gyromagnetic ratio. dGEMRIC provides an assessment of GAG concentration through the use of the intravenous negatively charged contrast agent $Gd(DTPA)^{2-}$, which distributes in cartilage in inverse relation to the negatively charged GAG concentration (13,14). dGEMRIC has high SNR and sensitivity to GAG content, but is invasive and requires long wait times following injection of contrast agent. $T_{1\rho}$ relaxation time mapping is another method that is sensitive to in vivo GAG and collagen content (15,16). In cartilage, the mechanisms of proton exchange and dipolar relaxations contribute to $T_{1\rho}$ relaxation and make it sensitive to matrix macromolecular content and structure. Whereas the low frequency exchange of –OH and –NH protons on the GAG chains with bulk water protons alter both T_2 and $T_{1\rho}$ relaxation times, the dominant dipolar interaction masks smaller changes in T_2 relaxation time caused by the exchange mechanism. Spin locking in the $T_{1\rho}$ experiment refocuses or attenuates the dipolar interactions and makes the $T_{1\rho}$ relaxation sensitive to other relaxation mechanisms such as low-frequency proton exchange (17,18). Although this allows $T_{1\rho}$ relaxation time mapping to assess GAG content without the need for invasive contrast agents or specialized hardware, this method is not as specific for GAG content as other MR methods.

Chemical exchange saturation transfer (CEST) is a new sensitivity enhancement mechanism used to indirectly detect metabolite content based on exchange-related properties (19,20). In a CEST experiment, saturated magnetization from exchangeable protons on a pool of biologic molecules is transferred to a much larger pool of bulk water protons (21). This reduction in water signal results in a concentration-dependent contrast in CEST water images. CEST has been used to measure contrast from numerous endogenous mobile proteins and metabolites (22–25) in biological tissue, including GAG content in cartilage using the exchange between hydroxyl (-OH) protons on GAG and bulk water protons (GagCEST) (26,27). One of the key concerns of current CEST imaging techniques is long imaging times, which often limits acquisition to a single slice (28). Single-slice assessment

may not fully describe the cartilage variation, may miss focal lesions, and may obscure longitudinal changes (29,30). Furthermore, GagCEST parameters, such as the time between magnetization preparations, the delay time following the readout, and number of CEST preparations per k-space readout, play a large role in GagCEST contrast and scan times but have received little attention in previous studies.

In this work, we develop a new multislice GagCEST acquisition strategy for rapid and volumetric acquisition of GagCEST maps in articular cartilage. We investigate the effect of various scan parameters on the measured GagCEST asymmetry ($GagCEST_{asym}$) to optimize the sequence for scan-time efficiency and maximize $GagCEST_{asym}$. To assess the feasibility of whole-joint GagCEST imaging in vivo, the optimized multislice GagCEST protocol was applied to GAG mapping of the ankle in healthy volunteers. Finally, to compare GAG distribution determined with our new GagCEST mapping technique to established methods, we compare the relationship between $GagCEST_{asym}$ with $T_{1\rho}$ relaxation times.

METHODS

Multislice CEST Sequence

The multislice CEST pulse sequence is shown in Figure 1. It consists of a frequency-selective saturation pulse followed by a chemical-shift-selective fat saturation pulse and a segmented radiofrequency (RF) spoiled gradient recalled echo (SPGR) acquisition with centric phase encoding and interleaved slice-encoding order. This magnetization preparation and readout is followed by a delay and is defined as a shot, which can be repeated for various scan parameters (eg, saturation frequency offsets, segmented k-space acquisitions, averages). To conform to scanner hardware limits, the saturation pulse consists of a train of Hanning-windowed rectangular pulses with short interpulse delays. In this study, a train of 100-ms pulses with a 99% duty cycle was used (99-ms pulse, 1-ms delay). For a saturation train duration of 500 ms, the saturation pulse excitation bandwidth (50%) is 10Hz with a 1% bandwidth of 40Hz. The readout acquisition acquired a single line of k-space from each slice before repeating the same slice again. As a result, the effective repetition time (TR) for each slice is the TR for each line multiplied by the number of slices. Centric phase encoding was used to allow the center of k-space to be acquired immediately after the CEST saturation pulse. Multiple partitions (magnetization preparations/multislice readout) could be used to segment k-space across multiple CEST magnetization preparations. Following saturation and acquisition of SPGR segments, a delay is added to allow for T_1 recovery. The same sequence with lower saturation power and shorter duration is used for water saturation shift reference (WASSR) data acquisition (31).

MR Imaging

All imaging experiments were performed on a 7 Tesla (T) whole body scanner (GE Healthcare, Milwaukee, Wisconsin) with a vendor-supplied 32-channel volume RF coil (Nova Medical, Wilmington, Massachusetts). CEST imaging experiments used a 500-ms saturation pulse train (100-ms pulses, 99% duty cycle) and a B_{1rms} of 77 Hz (1.8 μT). Other imaging parameters were: echo time (TE)/TR = 2.3/4.9 ms, eight slices, effective TR for each slice = 39.2 ms, flip angle = 12 °, slice thickness = 3 mm, field of view = 140 × 140

mm^2, matrix size = 192 × 192. GAG hydroxyl protons have a chemical shift of 1.0 ppm relative to the water resonance. Therefore, we acquired CEST images with varying saturation offsets from +0.6 to +1.4 ppm and from −0.6 to −1.4 ppm (relative to water resonance) in 0.13-ppm increments. To remove field-inhomogeneity-induced artifacts in GagCEST maps, B_1 and ΔB_0 field maps were acquired using the double angle and WASSR methods, respectively (31,32). For WASSR images, a 200-ms saturation pulse train with B_{1rms} of 12.4 Hz (0.3 μT) was used from −0.6 to 0.6 ppm.

Ex Vivo Bovine Knee Imaging

To assess the effect of the multislice GagCEST sequence on $GagCEST_{asym}$, an immature bovine knee specimen was imaged. Multislice CEST data from eight slices were acquired with a constant shot TR of 10 s, with 1 (2:20), 2 (4:40), 4 (9:20), and 8 (18:40) partitions (shots per k-space readout), and compared with a single-slice acquisition (2:20). Additionally, CEST scans with 1 partition were repeated with varying shot TR (8.2, 10, 12, and 15 s) to observe their effects on the computed $GagCEST_{asym}$.

In Vivo Ankle Imaging

All studies were conducted under a Stanford University– approved Institutional Review Board protocol. Informed consent from each volunteer was obtained after explaining the study protocol. CEST images were acquired from a healthy volunteer at varying saturation amplitude and duration to empirically optimize the saturation parameters for GagCEST in tibiotalar cartilage. Imaging of the ankle was then performed on 10 healthy controls (6 males, ages 23–51). Eight slices across the tibiotalar cartilage were acquired. For CEST imaging, two partitions were used with a shot TR of 8 s (total imaging time 3:44). Along with B_1 (0:20) and ΔB_0 (2:40) field maps, the total scan time was approximately 6 min, 44 s. Additionally, $T_{1\rho}$ mapping was performed on the same eight slices. $T_{1\rho}$ magnetization preparations used a 90 ° RF pulse followed by two rectangular spin-lock pulses and finally a 90 ° storing pulse. The spin-lock pulses are phase alternating, to refocus the effect of an inhomogeneous B_1 field (33). $T_{1\rho}$ imaging was performed with a spin-lock amplitude of 500 Hz at six spin-lock times (t_{SL}) (2–60 ms) followed by the same SPGR readout.

Analysis

All image processing and data analysis were performed using in-house written MATLAB (MathWorks, Natick, Massachusetts, version 8.2, R 2013b) scripts. A B_1 calibration curve for the cartilage tissue was developed from in vivo human tibiotalar cartilage CEST data at varying saturation amplitudes and used in conjunction with B_1 maps to correct for B_1 inhomogeneities. For both ex vivo and in vivo studies, cartilage was manually segmented from morphologic images for analysis. CEST data were corrected for B_0 and B_1 field inhomogeneities using the previously described methods (31,32), and the CEST asymmetry resulting from GAG was calculated using the equation

$$\mathrm{GagCEST}_{\mathrm{asym}} = \frac{S_{-1.0ppm} - S_{+1.0ppm}}{S_{-1.0ppm}}$$

where $S_{\pm 1ppm}$ is the B_0-corrected signal intensity of images acquired with saturation at ±1.0 ppm. Signal to noise ratio was computed as the signal from cartilage in B_0-corrected images acquired with saturation at +1.0 ppm (S_{+1ppm}) divided by the standard deviation of background noise in the images in which no signal was expected to be present. $T_{1\rho}$ maps were constructed by fitting image data at varying t_{SL} to the following equation:

$$S(t_{SL}) = S_0 e^{-(t_{SL}/T_{1\rho})}$$

The average $GagCEST_{asym}$ and standard deviation (SD) between slices was calculated for each subject. A coefficient of variation (SD/mean) was computed to observe the variation in $GagCEST_{asym}$ between slices. To compare $GagCEST_{asym}$ to $T_{1\rho}$ relaxation time, cartilage in each slice for each volunteer was manually segmented into anterior, medial, and posterior segments. The average $GagCEST_{asym}$ and $T_{1\rho}$ values in each of these segments were computed. A Pearson coefficient was computed to observe the correlation between GagCEST and $T_{1\rho}$.

RESULTS

Figure 2 shows B_0 and B_1-corrected $GagCEST_{asym}$ maps of bovine articular cartilage acquired with multislice acquisitions with different numbers of k-space partitions. Increasing the number of partitions, and thus decreasing the amount of k-space lines acquired following each CEST magnetization preparation, increased the measured GagCEST asymmetry. In the evaluated slice, the average $GagCEST_{asym}$ for one, two, four, and eight partitions were 18.3 ± 2.6%, 21.0 ± 2.5%, 22.0 ± 2.3%, and 22.4 ± 2.4%, respectively (Figs. 2a–2d). The average $GagCEST_{asym}$ in the cartilage for GagCEST acquired on a single slice was 19.2 ± 2.4% (Fig. 2e), which was higher than the average for one partition but lower than the average $GagCEST_{asym}$ values acquired with two or more partitions. Although the average $GagCEST_{asym}$ increased with the number of partitions, the distribution and standard deviation of $GagCEST_{asym}$ values within the segmented cartilage stayed relatively constant. Figure 2f shows the relationship between $GagCEST_{asym}$ and SNR of cartilage in B_0-corrected images acquired with a saturation at +1.0 ppm as a function of the number of partitions. The $GagCEST_{asym}$ and SNR followed a similar trend. Data about $GagCEST_{asym}$ and SNR acquired from a single slice were added as single points on the curve and correlated to $GagCEST_{asym}$ and SNR from approximately 1.3 partitions.

The effect of varying the repetition time between CEST magnetization preparations is shown in Figure 3. Increasing the shot TR resulted in increased $GagCEST_{asym}$. In the evaluated slice, the average $GagCEST_{asym}$ was 11.7 ± 2.7%, 17.9 ± 2.5%, 18.3 ± 2.5%, and 19.1 ± 2.4% for shot TRs of 8.2, 10, 12, and 15 s, respectively (Figs. 3a–3d). Again, the relationship between $GagCEST_{asym}$ and SNR is plotted as a function of shot TR and also follows a similar trend (Fig. 3e). Additionally, the association between $GagCEST_{asym}$ and time delay from the last acquired readout line and the start of the next CEST magnetization preparation for data acquired with varying partitions and shot TR is shown in Figure 3f.

All healthy volunteers had morphologically intact tibiotalar cartilage on proton-density-weighted MR images as judged by an experienced musculoskeletal radiologist. Figure 4

shows $GagCEST_{asym}$ maps of cartilage between the tibia and the talus for eight slices across the ankle joint of a healthy volunteer. A higher $GagCEST_{asym}$ was observed centrally in the cartilage. Figure 5 shows $GagCEST_{asym}$ maps (Fig. 5a) and $T_{1\rho}$ maps (Fig. 5b) of cartilage between the tibia and the talus in the ankle joint of a healthy volunteer. The cartilage was manually segmented into anterior, medial, and posterior segments (Fig. 5c), and the average $GagCEST_{asym}$ is plotted as a function of $T_{1\rho}$ relaxation time for each segment across eight slices in Figure 5d. For this healthy volunteer, a Pearson correlation coefficient of −0.85 was observed between $GagCEST_{asym}$ and $T_{1\rho}$ relaxation time.

For the 10 subjects with no observed cartilage lesions, the average $GagCEST_{asym}$ values stayed relatively constant across slices. A coefficient of variation of $GagCEST_{asym}$ across slices of less than 15% was observed for all healthy subjects, suggesting fairly uniform GAG content across the tibiotalar cartilage (Table 1). A similarly low coefficient of variation (<11%) was observed for $T_{1\rho}$ relaxation times across slices. Across the 10 subjects, the average $GagCEST_{asym}$ was 8.8 ± 0.7%, whereas the average $T_{1\rho}$ relaxation time was 49.6 ± 2.5 ms. The average $GagCEST_{asym}$ as a function of $T_{1\rho}$ relaxation times for cartilage segmented into anterior, medial, and posterior sections across eight slices for all 10 subjects is shown in Figure 6. Across subjects, there was a Pearson correlation coefficient of −0.58 observed between measured $gagCEST_{asym}$ and $T_{1\rho}$ relaxation times.

DISCUSSION

The results of this work demonstrate the feasibility and optimization of multislice GagCEST mapping of articular cartilage. GagCEST contrast from a bovine knee specimen showed that $GagCEST_{asym}$ contrast acquired on eight slices simultaneously was comparable in distribution to that of a single-slice acquisition. Furthermore, the measured $GagCEST_{asym}$ in cartilage was higher in multislice acquisitions with two or more partitions than with single-slice acquisition. This is likely the result of the increase in SNR of CEST magnetization-prepared images. As slice acquisition is interleaved, the effective TR during acquisition for each slice was 39.2 ms (TR × number of slices), resulting in increased SNR. Centric encoding and multiple partitions meant CEST information following the saturation pulse was acquired for low spatial frequencies (center of k-space) well before the cartilage longitudinal relaxation was able to occur, thus preserving CEST contrast.

Ex vivo data also showed that the number of partitions and delay times play a role in the $GagCEST_{asym}$ values. Although the GagCEST contrast was similar, $GagCEST_{asym}$ values increased with an increasing number of partitions. The reasons for this are two-fold. First, increasing the number of partitions results in k-space acquisition closer to the CEST magnetization preparation. Although this reduces the CEST contrast in high spatial frequencies, only a small effect is observed on the overall $GagCEST_{asym}$ as low spatial frequencies, which are responsible for most of the SNR that are still acquired close to the CEST magnetization preparation. An increase in $GagCEST_{asym}$ of 1.4% (6.25% of the total $GagCEST_{asym}$) was obtained when the number of partitions was increased from two to eight. However, the acquisition time increased proportionally to the number of partitions, and thus took four times longer to acquire images with eight partitions than with two partitions.

The other reason $GagCEST_{asym}$ values increased with an increasing number of partitions relates to shot TR. A long shot TR allows for recovery of magnetization following the saturation pulse and recovery of the magnetization at the end of the SPGR readout. Because greater than 192 readout lines are being acquired per each CEST magnetization preparation in all scans performed in this study, we are constrained primarily by the post readout delay. This is shown in Figure 3. At 7T, the T_1 of cartilage is approximately 1500 ms; thus, a 7.5-s delay from one CEST saturation pulse to the start of the next one (8 s total) would result in a 99.4% recovery of the saturated magnetization. However, it appears that the $GagCEST_{asym}$ and SNR are considerably reduced when the shot TR is 8200 ms. This is because with one partition, the CEST saturation and SPGR readout require over 8000 ms, leaving less than 200 ms for recovery of the steady-state SPGR signal. However, we see that above 2000 ms, increasing the post readout delay has a minimal effect on the $GagCEST_{asym}$, while greatly increasing the scan time.

To balance the acquisition time with the integrity of signal from layers of cartilage, two partitions with a shot TR of 8000 ms were used for our in vivo study. This creates for a 7500-ms gap between CEST magnetization preparations and a 3700-ms post readout delay, which allowed our multislice GagCEST sequence to acquire all of the data (CEST, B0, B1) needed to generate high-resolution and high-SNR $GagCEST_{asym}$ maps of tibiotalar cartilage in less than 7 min. Additionally, the long delay allows for full magnetization recovery and higher $GagCEST_{asym}$ compared with the currently used volumetric 3D GagCEST sequence (27), which uses short shot TRs that result in substantially lower starting magnetizations and therefore lower SNR.

There was good agreement between $GagCEST_{asym}$ maps and $T_{1\rho}$ relaxation maps. Depletion of proteoglycans, and thus GAG, results in increased $T_{1\rho}$ relaxation times. As expected, higher $GagCEST_{asym}$ appeared to correlate with lower $T_{1\rho}$ values in our volunteers. It should be noted that the cartilage between the tibia and the talus consists of two layers of cartilage separated by joint fluid. However, the layer of joint fluid is thin and is not expected to exhibit a CEST effect, and thus should not be expected to influence the $GagCEST_{asym}$ maps. For the 10 subjects with no observed cartilage lesions studied, the average $GagCEST_{asym}$ values stayed relatively constant across slices, suggesting fairly uniform GAG content across the tibiotalar cartilage (Table 1). Across the 10 subjects and eight slices per subjects, there was a Pearson correlation of $r = -0.58$ observed between the measured $GagCEST_{asym}$ and $T_{1\rho}$ relaxation times, demonstrating some negative correlation. Similar to GagCEST, proton exchange between GAG hydroxyl protons and bulk water also contributes to $T_{1\rho}$ relaxation (34). However, although $GagCEST_{asym}$ is thought to be affected primarily by GAG concentration, $T_{1\rho}$ relaxation is also influenced by dipolar relaxation and translational diffusion, and has been shown to be affected by collagen content and orientation in addition to GAG content, which may affect the correlation.

There are several potential limitations in this study. For comparison purposes, single-slice CEST data were acquired with the same flip angle used for multislice acquisitions. As discussed previously, because the effective TR of the SPGR for the single-slice readout was eight times shorter than that for the multislice readout, this flip angle was likely higher than the optimal flip angle to maximize the SNR and measured $GagCEST_{asym}$ in the single-slice

acquisition. Furthermore, the slice thickness used for imaging of tibiotalar cartilage may have resulted in partial volume effects, which may have influenced measurements of $GagCEST_{asym}$ and $T_{1\rho}$ relaxation times, particularly at boundaries between bone and cartilage. Similarly, partial volume effects in thinner areas of cartilage could also effect measured values. Additionally, while B_1 inhomogeneities are corrected for in $GagCEST_{asym}$ maps, they are not accounted for in $T_{1\rho}$ relaxation times. Variation in B_1 results in higher or lower spinlock amplitudes, which directly affects the $T_{1\rho}$ relaxation time. This may have affected the correlation between $GagCEST_{asym}$ and $T_{1\rho}$ relaxation times. However, the standard deviation of B_1 values in the tibiotalar cartilage was kept below 10% and is not expected to have a large effect on the measured $T_{1\rho}$ relaxation times.

In summary, this work demonstrated the feasibility of rapid volumetric GagCEST mapping of articular cartilage. It was shown that shot TR and the number of partitions are important parameters that must be optimized to balance maximizing $GagCEST_{asym}$ and scan time. Ex vivo experiments were used to observe the effect of the number of partitions and shot TR on SNR and measured $GagCEST_{asym}$. These results were incorporated into the optimization of scan parameters, to perform GagCEST imaging of the entire tibiotalar ankle joint in under 7min. Measured $GagCEST_{asym}$ was compared with $T_{1\rho}$ relaxation times, and a negative correlation was observed as expected. Higher SNR was observed, compared with single-slice acquisitions, which may be beneficial for GagCEST imaging at lower field strengths. Future work to incorporate parallel imaging to further decrease scan times or increase the CEST contrast at higher spatial frequencies would help advance the clinical utility of GagCEST imaging of articular cartilage and allow for whole-joint imaging of larger joints, such as the knee, in more reasonable scan times.

REFERENCES

1. Sarzi-Puttini, P., Cimmino, MA., Scarpa, R., Caporali, R., Parazzini, F., Zaninelli, A., Atzeni, F., Canesi, B. Osteoarthritis: An Overview of the Disease and Its Treatment Strategies. Philadelphia, PA: Elsevier; 2005. p. 1-10.
2. Arden N, Nevitt MC. Osteoarthritis: epidemiology. Best Pract Res Clinic Rheumatol. 2006; 20(1):3–25.
3. Hiligsmann M, Cooper C, Arden N, et al. Health economics in the field of osteoarthritis: an expert's consensus paper from the European Society for Clinical and Economic Aspects of Osteoporosis and Osteoarthritis (ESCEO). Sem Arthritis Rheum. 2013; 43(3):303–313.
4. Peterfy CG, Guermazi A, Zaim S, et al. Whole-Organ Magnetic Resonance Imaging Score (WORMS) of the knee in osteoarthritis. Osteoarthr Cartilage. 2004; 12(3):177–190.
5. Eckstein F, Burstein D, Link TM. Quantitative MRI of cartilage and bone: degenerative changes in osteoarthritis. NMR Biomed. 2006; 19(7):822–854. [PubMed: 17075958]
6. Malemud CJ. Changes in proteoglycans in osteoarthritis: biochemistry, ultrastructure and biosynthetic processing. J Rheumatol Suppl. 1991; 27:60–62. [PubMed: 2027133]
7. Guermazi A, Burstein D, Conaghan P, Eckstein F, Hellio Le Graverand-Gastineau MP, Keen H, Roemer FW. Imaging in osteoarthritis. Rheum Dis Clin North Am. 2008; 34(3):645–687. [PubMed: 18687277]
8. Stahl R, Luke A, Li X, Carballido-Gamio J, Ma CB, Majumdar S, Link TM. T1rho, T2 and focal knee cartilage abnormalities in physically active and sedentary healthy subjects versus early OA patients—a 3.0-Tesla MRI study. Eur Radiol. 2009; 19(1):132–143. [PubMed: 18709373]
9. Matzat SJ, Kogan F, Fong GW, Gold GE. Imaging strategies for assessing cartilage composition in osteoarthritis. Curr Rheumatol Rep. 2014; 16(11):462. [PubMed: 25218737]

10. Li X, Majumdar S. Quantitative MRI of articular cartilage and its clinical applications. J Magn Reson Imaging. 2013; 38(5):991–1008. [PubMed: 24115571]
11. Madelin G, Babb J, Xia D, Chang G, Krasnokutsky S, Abramson SB, Jerschow A, Regatte RR. Articular cartilage: evaluation with fluid-suppressed 7.0-T sodium MR imaging in subjects with and subjects without osteoarthritis. Radiology. 2013; 268(2):481–491. [PubMed: 23468572]
12. Wheaton AJ, Borthakur A, Shapiro EM, Regatte RR, Akella SV, Kneeland JB, Reddy R. Proteoglycan loss in human knee cartilage: quantitation with sodium MR imaging—feasibility study. Radiology. 2004; 231(3):900–905. [PubMed: 15163825]
13. Tiderius CJ, Olsson LE, Leander P, Ekberg O, Dahlberg L. Delayed gadolinium-enhanced MRI of cartilage (dGEMRIC) in early knee osteoarthritis. Magn Reson Med. 2003; 49(3):488–492. [PubMed: 12594751]
14. Ericsson YB, Tjornstrand J, Tiderius CJ, Dahlberg LE. Relationship between cartilage glycosaminoglycan content (assessed with dGEMRIC) and OA risk factors in meniscectomized patients. Osteoarthr Cartilage. 2009; 17(5):565–570.
15. Borthakur A, Mellon E, Niyogi S, Witschey W, Kneeland JB, Reddy R. Sodium and T1rho MRI for molecular and diagnostic imaging of articular cartilage. NMR Biomed. 2006; 19(7):781–821. [PubMed: 17075961]
16. Singh A, Haris M, Cai K, Kogan F, Hariharan H, Reddy R. High resolution T1rho mapping of in vivo human knee cartilage at 7T. PloS One. 2014; 9(5):e97486. [PubMed: 24830386]
17. Akella SV, Regatte RR, Wheaton AJ, Borthakur A, Reddy R. Reduction of residual dipolar interaction in cartilage by spin-lock technique. Magn Reson Med. 2004; 52(5):1103–1109. [PubMed: 15508163]
18. Chaumette H, Grandclaude D, Canet D. Rotating-frame spin-lattice relaxation time imaging by radio-frequency field gradients: visualization of strained crosslinked natural rubbers. J Magn Reson. 2003; 163(2):369–373. [PubMed: 12914854]
19. Guivel-Scharen V, Sinnwell T, Wolff SD, Balaban RS. Detection of proton chemical exchange between metabolites and water in biological tissues. J Magn Reson. 1998; 133(1):36–45. [PubMed: 9654466]
20. van Zijl PC, Yadav NN. Chemical exchange saturation transfer (CEST): what is in a name and what isn't? Magn Reson Med. 2011; 65(4):927–948. [PubMed: 21337419]
21. Kogan F, Hariharan H, Reddy R. Chemical Exchange Saturation Transfer (CEST) imaging: description of technique and potential clinical applications. Curr Radiol Rep. 2013; 1(2):102–114. [PubMed: 23730540]
22. Kogan F, Haris M, Singh A, Cai K, Debrosse C, Nanga RP, Hariharan H, Reddy R. Method for high-resolution imaging of creatine in vivo using chemical exchange saturation transfer. Magn Reson Med. 2014; 71(1):164–172. [PubMed: 23412909]
23. Cai K, Haris M, Singh A, Kogan F, Greenberg JH, Hariharan H, Detre JA, Reddy R. Magnetic resonance imaging of glutamate. Nature Med. 2012; 18(2):302–306. [PubMed: 22270722]
24. Dula AN, Dewey BE, Arlinghaus LR, Williams JM, Klomp D, Yankeelov TE, Smith S. Optimization of 7-T chemical exchange saturation transfer parameters for validation of glycosaminoglycan and amide proton transfer of fibroglandular breast tissue. Radiology. 2015; 275(1):255–261. [PubMed: 25353249]
25. Zhou J, Tryggestad E, Wen Z, et al. Differentiation between glioma and radiation necrosis using molecular magnetic resonance imaging of endogenous proteins and peptides. Nature Med. 2011; 17(1):130–134. [PubMed: 21170048]
26. Ling W, Regatte RR, Navon G, Jerschow A. Assessment of glycosaminoglycan concentration in vivo by chemical exchange-dependent saturation transfer (gagCEST). Proc Nat Acad Sci. 2008; 105(7):2266. [PubMed: 18268341]
27. Schmitt B, Zbyn S, Stelzeneder D, Jellus V, Paul D, Lauer L, Bachert P, Trattnig S. Cartilage quality assessment by using glycosaminoglycan chemical exchange saturation transfer and (23)Na MR imaging at 7T. Radiology. 2011; 260(1):257–264. [PubMed: 21460030]
28. Singh A, Haris M, Cai K, Kassey VB, Kogan F, Reddy D, Hariharan H, Reddy R. Chemical exchange saturation transfer magnetic resonance imaging of human knee cartilage at 3 T and 7T. Magn Reson Med. 2012; 68(2):588–594. [PubMed: 22213239]

29. Carballido-Gamio J, Bauer JS, Stahl R, Lee KY, Krause S, Link TM, Majumdar S. Inter-subject comparison of MRI knee cartilage thickness. Med Image Anal. 2008; 12(2):120–135. [PubMed: 17923429]

30. Carballido-Gamio J, Joseph GB, Lynch JA, Link TM, Majumdar S. Longitudinal analysis of MRI T2 knee cartilage laminar organization in a subset of patients from the osteoarthritis initiative: a texture approach. Magn Reson Med. 2011; 65(4):1184–1194. [PubMed: 21413082]

31. Kim M, Gillen J, Landman BA, Zhou J, van Zijl PC. Water saturation shift referencing (WASSR) for chemical exchange saturation transfer (CEST) experiments. Magn Reson Med. 2009; 61(6): 1441–1450. [PubMed: 19358232]

32. Singh A, Cai K, Haris M, Hariharan H, Reddy R. On B1 inhomogeneity correction of in vivo human brain glutamate chemical exchange saturation transfer contrast at 7T. Magn Reson Med. 2013; 69(3):818–824. [PubMed: 22511396]

33. Witschey WR, Borthakur A, Elliott MA, Mellon E, Niyogi S, Wang C, Reddy R. Compensation for spin-lock artifacts using an off-resonance rotary echo in T1rhooff-weighted imaging. Magn Reson Med. 2007; 57(1):2–7. [PubMed: 17191245]

34. Mlynarik V, Szomolanyi P, Toffanin R, Vittur F, Trattnig S. Transverse relaxation mechanisms in articular cartilage. J Magn Reson. 2004; 169(2):300–307. [PubMed: 15261626]

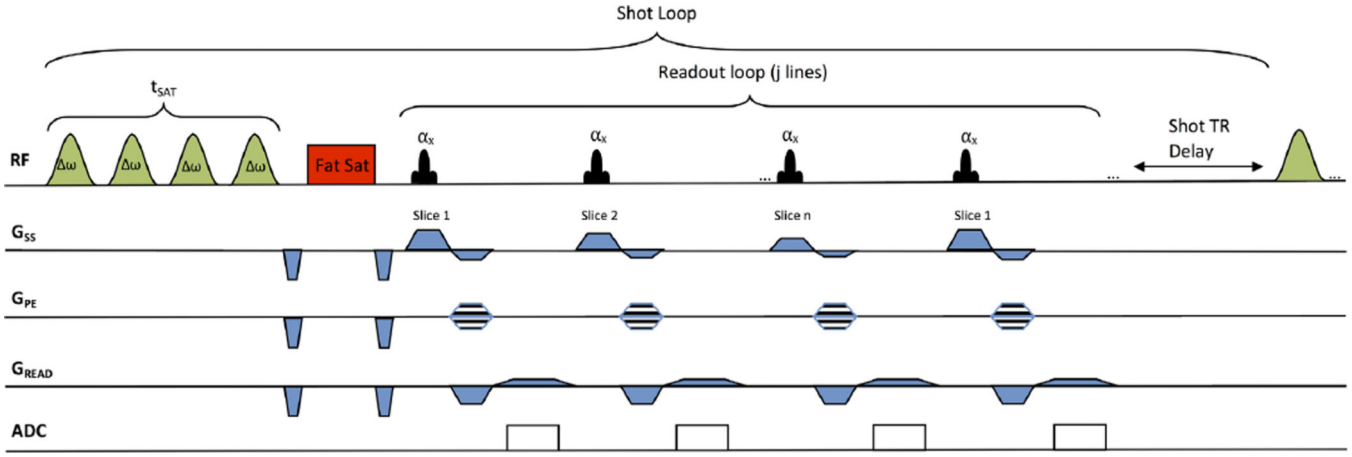

FIG. 1.

Pulse sequence diagram for a multislice, CEST-prepared sequence. CEST magnetization preparation involves a frequency-selective saturation pulse consisting of a train of Hanning windowed rectangular pulses with short interpulse delays. This is followed by a chemical shift selective fat saturation pulse and a segmented radiofrequency spoiled gradient recalled readout (SPGR) acquisition with centric phase and interleaved slice-encoding order. The readout acquisition acquires a single line of k-space from each slice before repeating a different k-space line for the same slice again. Multiple partitions (magnetization preparations/multislice readout) could be used to segment k-space across multiple CEST magnetization preparations. The number of k-space lines (*j*) acquired for each magnetization preparation is equal to the number of phase encodes multiplied by the number of slices (*n*) and divided by the number of partitions. Following saturation and acquisition of SPGR segments, a delay is added to allow for T_1 recovery.

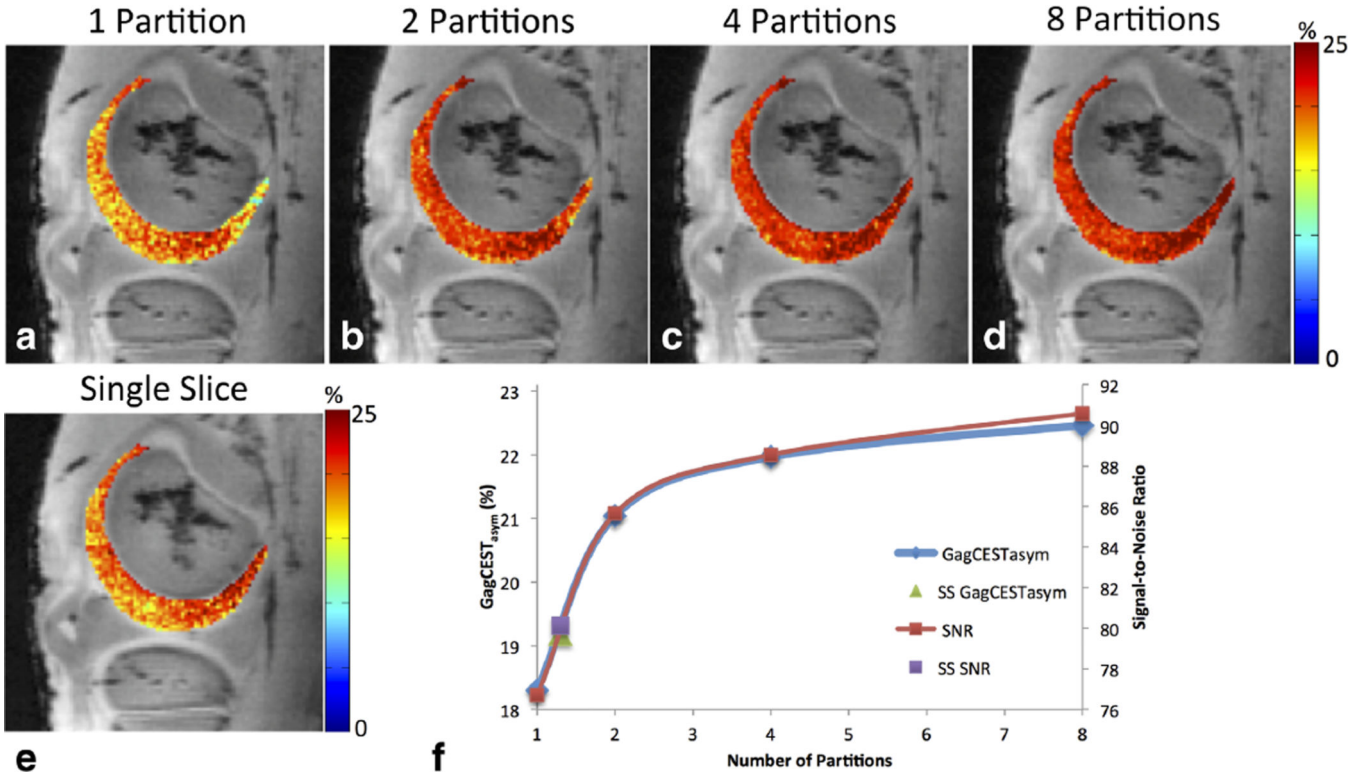

FIG. 2.

B_0 and B_1 corrected GagCEST$_{asym}$ maps of bovine articular cartilage acquired with one (a), two (b), three (c), and four (d) k-space partitions, as well as with single-slice (SS) acquisition (e). Plot (f) shows the relationship between GagCEST$_{asym}$ and SNR of cartilage in B_0-corrected images acquired with saturation at +1.0 ppm as a function of number of partitions, with single-slice-acquisition GagCEST$_{asym}$ and SNR data added as single points on the curve. The single-slice data correlate to multislice GagCEST$_{asym}$ and SNR from approximately 1.3 partitions.

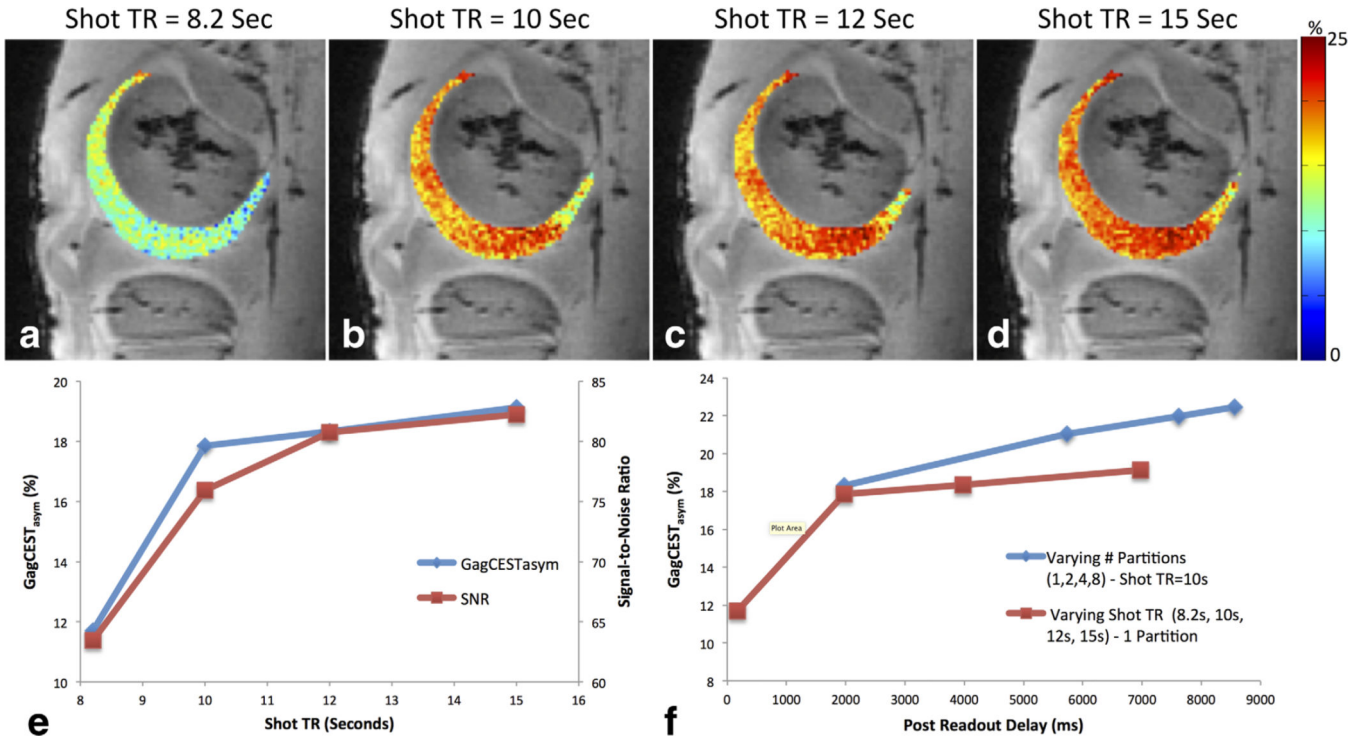

FIG. 3.

Effect of varying the repetition time between CEST magnetization preparations. B_0 and B_1-corrected GagCEST$_{asym}$ maps of bovine articular cartilage are shown acquired with a shot TR of 8.2 (a), 10 (b), 12 (c), and 15 (d) seconds. The relationship between GagCEST$_{asym}$ and SNR is plotted as a function of shot TR (e) and the association between GagCEST$_{asym}$ and time delay from the last acquired readout line to the start of the next CEST magnetization preparation for data acquired with varying partitions and shot TR is shown in (f).

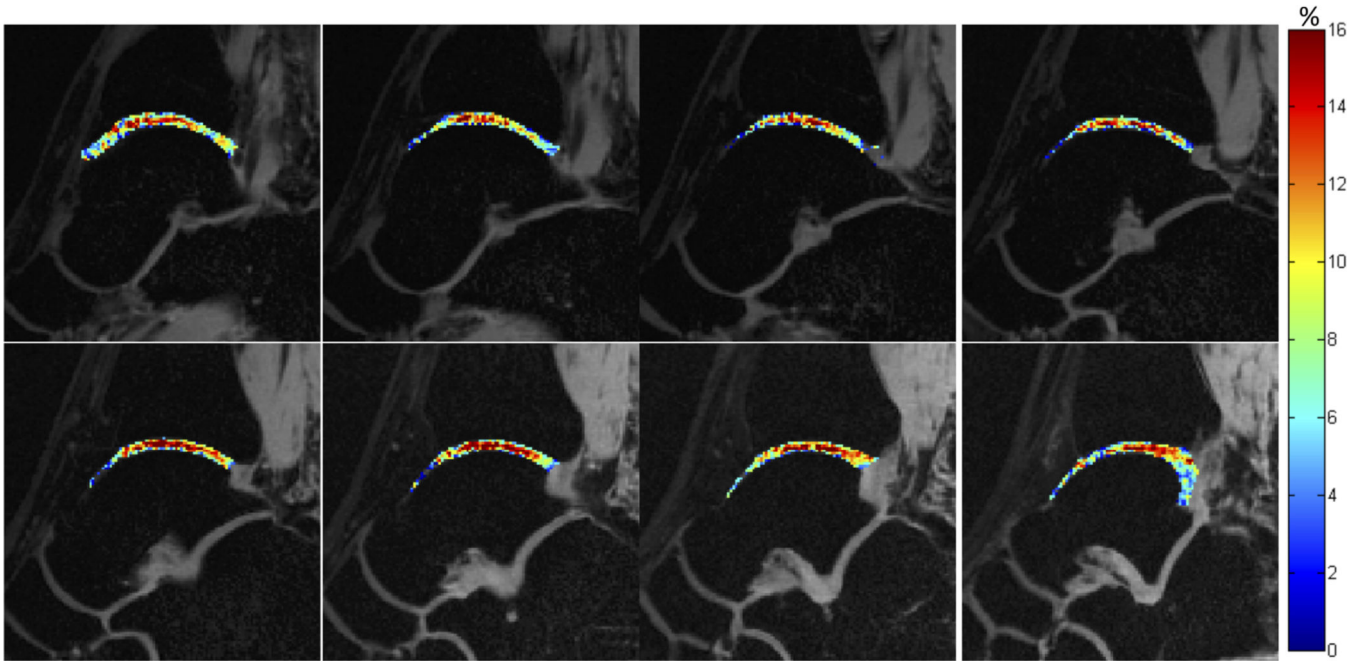

FIG. 4.

GagCEST$_{asym}$ maps of cartilage between the tibia and the talus for eight slices across the ankle joint of a healthy volunteer.

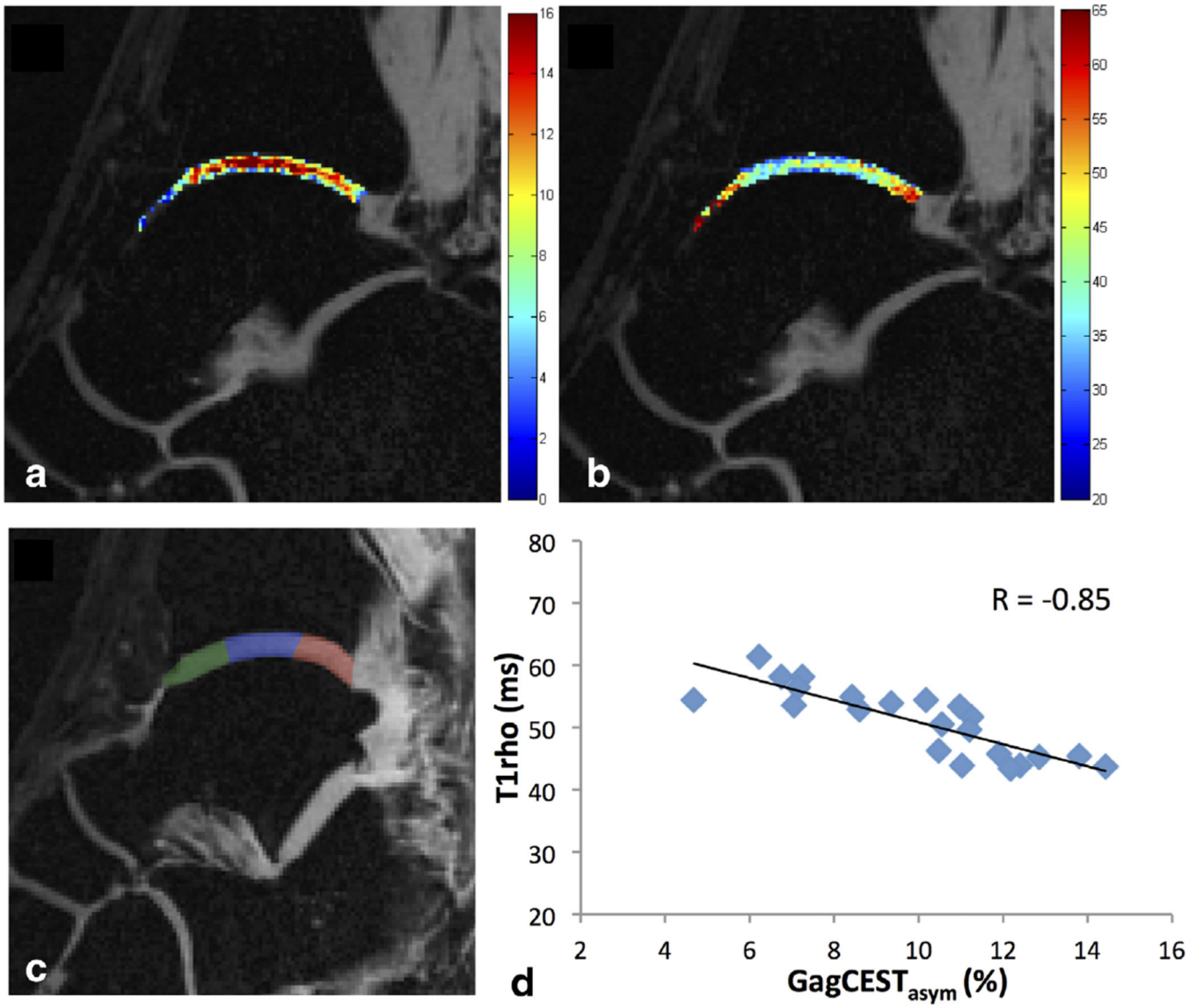

FIG. 5.

GagCEST$_{asym}$ maps (a) and $T_{1\rho}$ maps (b) of cartilage between the tibia and the talus in the ankle joint of a healthy volunteer. The cartilage was manually segmented into anterior (green), medial (blue), and posterior (red) segments (c), and the average GagCEST$_{asym}$ is plotted as a function of $T_{1\rho}$ relaxation time for each segment across eight slices (d). For this healthy volunteer, a Pearson correlation coefficient of −0.85 was observed between GagCEST$_{asym}$ and $T_{1\rho}$ relaxation time.

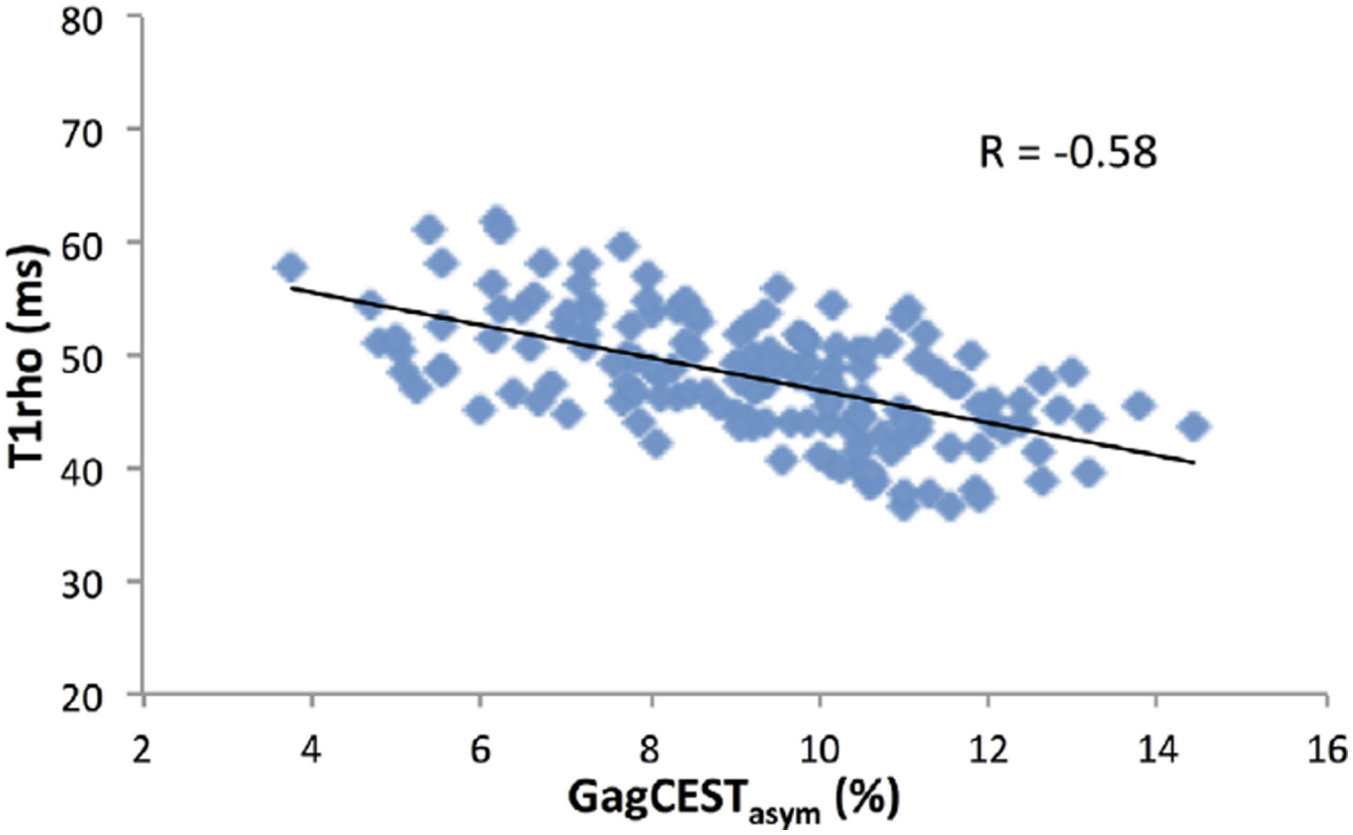

FIG. 6.

Average $GagCEST_{asym}$ as a function of $T_{1\rho}$ relaxation times for cartilage segmented into anterior, medial, and posterior sections across eight slices for all 10 subjects. Across subjects, there was a Pearson correlation coefficient of −0.58 observed between the measured $gagCEST_{asym}$ and $T_{1\rho}$ relaxation times.

Table 1

Average GagCEST$_{asym}$ and $T_{1\rho}$ Relaxation Times and Variation Across Slices for 10 Healthy Subjects

Subject	GagCESTasym (mean (SD)) %	cv (SD/Mean)	Tlrho (mean (SD)) ms	CV (SD/Mean)
1	9.4 (0.7)	0.08	47.7 (1.8)	0.04
2	8.9 (1.3)	0.15	46.5 (2.6)	0.06
3	9.0 (0.9)	0.10	48.3 (3.1)	0.06
4	8.0 (0.9)	0.11	51.8(2.2)	0.04
5	7.9 (0.3)	0.04	54.3 (3.1)	0.06
6	9.5 (1.1)	0.12	51.4(1.8)	0.03
7	10 (1.0)	0.10	49.7 (5.6)	0.11
8	7.9 (1.0)	0.13	46.4 (3.6)	0.08
9	8.9 (0.8)	0.09	51.6(0.5)	0.01
10	8.3 (1.0)	0.13	47.8 (2.6)	0.05